

DYNAMICAL ANALYSIS OF A CONSTRAINED FLEXIBLE EXTENSIBLE LINK WITH RIGID SUPPORT AND CLEARANCE

MIHAI DUPAC

School of Design, Engineering and Computing Bournemouth University, Dorset, United Kingdom
e-mail: mdupac@bournemouth.ac.uk

Dynamic response of robotic systems is affected by deformation of their flexible components, velocity and mass of the systems, as well as by the presence of clearance or impact between the components. Since accurate simulations of such robotic systems are increasingly important, the modelling and dynamical behaviour of an extensible mechanism with a rigid crank and a flexible link is investigated in this paper. The equations of motion of the extensible flexible link, constrained to a circular, Cartesian, elliptical, Cassinian, Lamé or pear-shaped quartic path, are presented. A dynamical analysis is carried out in order to compare the dynamical response of the flexible link vs. a rigid link under the combined effect of different parameters such as flexibility and clearance. The simulation result shows clear trajectories divergence due to the impact effect of the flexible link on the rigid crank.

Keywords: multibody dynamics, impact analysis, contact forces

1. Introduction

The modelling, simulation and control of mechanical and robotic systems have been frequently studied for several years. For the study of their dynamical properties, mechanical models containing rigid links connected by joints are considered. Their dynamical response is usually affected by deformation of the links, by the presence of clearance in the joints as well as by the impact of the components/links. All the mentioned factors affect system performance, which results in a low ability to perform high-precision manipulation, increased vibration and high levels of noise. Moreover, the dynamical stress caused by the motion and the impact of the links affects vibration characteristics of the mechanical system, and can make the linkage fail. However, small amount of information to date about constrained extensible flexible systems can be found in the literature, so any relevant contribution to the topics in particular and knowledge in general may be considered important.

Some classical examples of the modelling and simulation of flexible systems, their forward, inverse and impulsive dynamics, and their stability were discussed by Garcia and Bayo (1994), Beale *et al.* (1998), Kvecses and Cleghorn (2004). The kinematics and equilibrium of an extensible rod under axial load was presented in Filipich and Rosales (2000). Dynamic analysis of planar mechanisms with rotating slider joint and clearance received attention in Stoenescu and Marghitu (2003), and the simulation of the non-smooth translational joints with clearance was considered in the work of Zhuang and Wang (2012). In Rubinstein (1999), Dupac and Marghitu (2006), a dynamical analysis of some systems with lumped masses was considered. The effect of clearance and cracks on some lumped mass systems and the impact equations using Newton's law were discussed by Brach (1989), Dupac and Beale (2010). The modelling and simulation of impacting systems as well as the study of some contact force models were considered in Lankarani and Nikravesh (1990), Dupac and Beale (2010), Flores *et al.* (2010, 2011), Machado *et al.* (2012).

The control (by suppressing oscillations) of systems undergoing rotations and impacts, and periodic impacts between elastic beams and rigid beams was studied in Boghiu *et al.* (1996), Marghitu *et al.* (1999). A study concerning the free vibration of an extensible rotating beam was presented in the work of Leea and Sheub (2007). Combined vibration control of a flexible linkage mechanism for suppressing its vibrations and impact effects, as well as impact control in the case of a flexible link were discussed by Izumi and Hitaka (1993), Jin *et al.* (2004). The impact dynamics and control of flexible-joint and dual-arm robots were simulated in Zhang and Angeles (2005), Liu *et al.* (2007), and some systems with extensible members were studied by Fritzkowski and Kaminski (2009), Dupac (2012, 2013).

In this paper, the modelling and simulation of an extensible mechanism with a rigid crank and a flexible link constrained to follow a specific path was considered. Accurate simulations for some constrained trajectories, i.e., circular, Cartesian, elliptical, Cassinian, Lamé or pear-shaped quartic, explored mechanism behaviour under the combined effect of different parameters such as flexibility, impact due to clearance, and trajectory constraints. A dynamical analysis was carried out in order to compare the dynamical behaviour of the extensible mechanism with a flexible link vs. rigid link behaviour.

2. System model

In this section, a flexible extensible link which rotates about the “fixed end” C is considered. The extensible link is composed of a rigid guide of length l_{CQ} (having its “left” end denoted by C and its “right” end denoted by Q), and a moving part (flexible link) which in an un-deformed state has the length l_{AS} . A motor torque \mathbf{M}_1 acts on the rigid guide of the mechanical system.

The flexible link slides inside the guide CQ and has its “left” end denoted by A and its “right” end denoted by S as shown in Fig. 1. The distance between the left end C of the guide and the left end A of the slider (moving part) is denoted by l and represent the constrained trajectory of the end A of the flexible link.

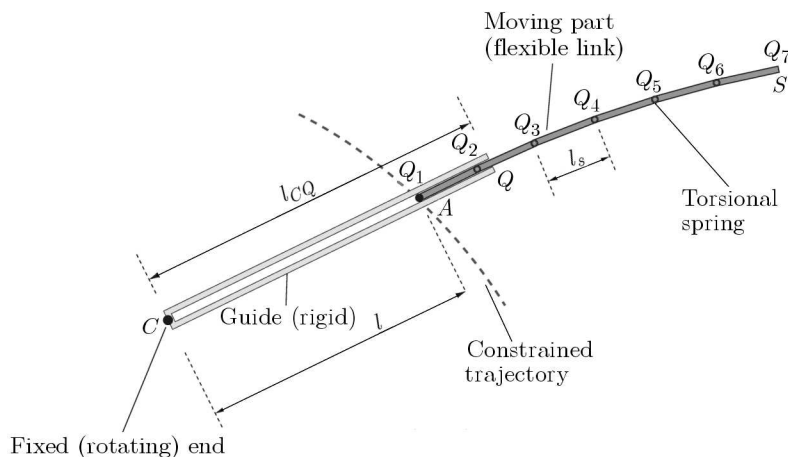


Fig. 1. Constrained flexible extensible link with rigid support model

2.1. Flexible link model

For the study of the flexible extensible mechanism with a rigid crank, a mechanical model similar to the one described by Dupac and Marghitu (2006), Dupac and Beale (2010) and shown in Fig. 2 is considered. The flexible link is modelled as a mechanical system with rigid rods connected by torsional springs.

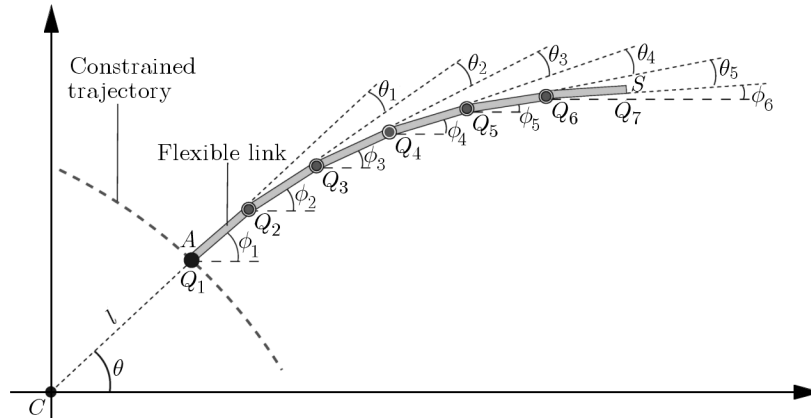


Fig. 2. Mechanical model of the flexible link modelled using n successive equal rigid rods $Q_i Q_{i+1}$, $i = \overline{1, n}$, the absolute angles ϕ_i and relative angles θ_i between two successive links

The flexible link shown in Fig. 2 is modelled using $n = 6$ successive equal rigid rods denoted by $Q_i Q_{i+1}$, $i = \overline{1, n}$, connected with torsional springs. Each one of the rods $Q_i Q_{i+1}$ has the mass $m_i = m$ and moment of inertia J . The spring constant used to model link flexibility is computed using Rubinstein (1999), Mitiguy and Banerjee (2000), as $k_s = EJ/l_{AS}$, where E is the Young modulus and $l_{AS} = \sum_{i=1}^n l_{Q_i Q_{i+1}}$ is the length of the flexible link AS when the link is not deformed. The rod $Q_1 Q_2$ is linked to the constrained trajectory with a slot-joint at Q_1 .

Each one of the rods $Q_i Q_{i+1}$, $i = \overline{1, n}$, has the length $l_{Q_i Q_{i+1}} = l_{AS}/n$. The angles θ_i , $i = \overline{1, n-1}$, represent the relative angle between the links $Q_i Q_{i+1}$ and $Q_{i+1} Q_{i+2}$. The angles between the link $Q_i Q_{i+1}$ and the horizontal direction denoted by ϕ_i are named the absolute angles. The system of two successive rods $Q_i Q_{i+1}$ and $Q_{i+1} Q_{i+2}$, and the corresponding moments M_i , M_{i+1} and M_{i+2} at the nodes Q_i , Q_{i+1} and Q_{i+2} , are presented in Fig. 3.

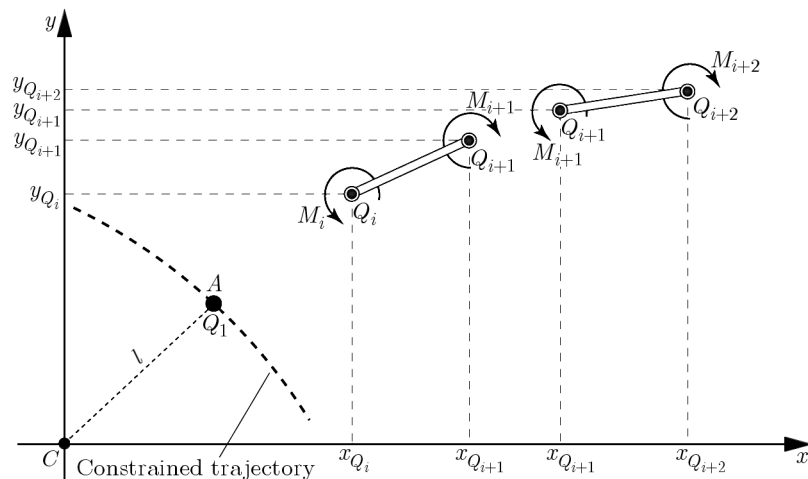


Fig. 3. System of two successive links $Q_i Q_{i+1}$ and $Q_{i+1} Q_{i+2}$ and their associated moments M_i , M_{i+1} , M_{i+2} at the corresponding nodes Q_i , Q_{i+1} , Q_{i+2}

2.2. Constrained trajectories of the flexible link

The end A of the flexible link (moving part) is constrained to follow one of the constrained trajectories shown in Fig. 4, that is, a circular, Cassinian, Cartesian (called also Descartes), elliptic, Lamé (also known as a super ellipse) or a pear-shaped quartic trajectory respectively.

One can see that the left end C of the guide shown in Fig. 4 is not the same as the center O of the constrained trajectories to which the end A is constrained. The extensible link shown

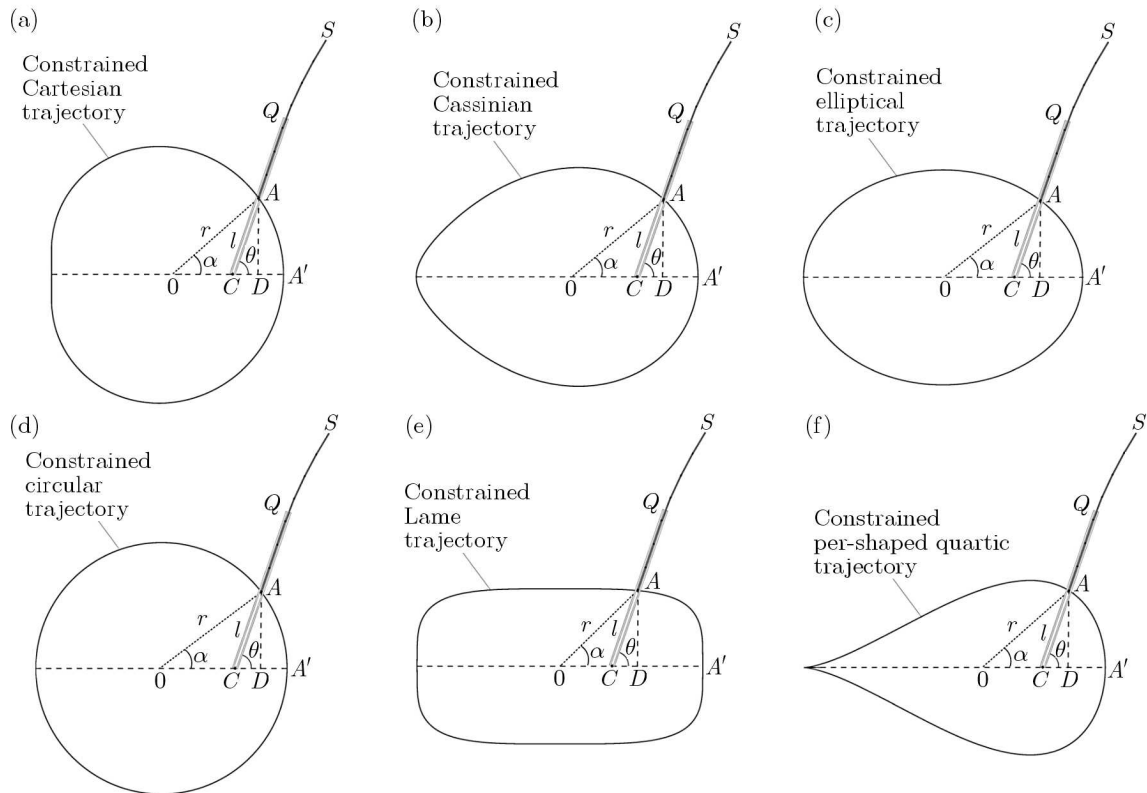


Fig. 4. Constrained flexible extensible link about: (a) Cartesian (called also Descartes), (b) Cassinian, (c) elliptical, (d) circular, (e) Lamé, (f) pear-shaped quartic trajectory

in Fig. 4, composed by the guide CQ and flexible link AS has the end C of the guide located on the Ox axis, the end A of the flexible link follows the constrained trajectory, distance d_{CA} between the end C and the left end A equal to l , i.e., $d_{CA} = l$, and the length between the end C and point A' denoted by $d_{CA'}$ equal to d .

Since it is important to describe the motion so that the point C represents the origin of the motion, a geometrical method developed in Dupac (2012, 2013), has been used to derive the associated equations of motion. The general Cartesian and polar equations of motion for all the circular, Cassinian, Cartesian, elliptical, Lamé and pear-shaped quartic trajectories are shown in Table 1.

The parameters for the Cartesian equations in Table 1 are defined as: a , b and c are real numbers, n is a natural number, and r is the distance between the center O of the Cartesian reference frame and the “left end” A of the flexible link. The parameters for the polar equations in Table 1 are defined as: a , b , c , d and m are real numbers, n_1 , n_2 and n_3 are natural numbers, r is the distance between the center O of the Cartesian reference frame and the “left end” A of the flexible link, α is the angle between Ox axis and the radius, and θ is the angle between the Ox axis and the rigid crank.

3. Dynamic model of the flexible link

The position vector of the center of mass W_i of each rigid rod Q_iQ_{i+1} , $i = \overline{1, n}$ of the constrained flexible extensible link is given by $\mathbf{r}_{W_i} = x_{W_i}\mathbf{i} + y_{W_i}\mathbf{j}$, where \mathbf{i} and \mathbf{j} are the unit vectors of the associated Cartesian reference frame Oxy . The horizontal and the vertical coordinates of the center of mass for each rod $i = \overline{1, n}$ can be expressed as

Table 1. Cartesian equations of motion for six possible constrained trajectories

Constrained trajectory	Cartesian equation	Polar equation
Circular	$(x - a)^2 + (y - b)^2 = r^2$	$l^2 = r^2 + (r - d)^2 - 2r(r - d) \frac{l \cos \theta + (r - d)}{r}$
Elliptical	$\left(\frac{x}{a}\right)^2 + \left(\frac{y}{b}\right)^2 = 1$	$l = \frac{b^2}{a - \cos(\pi - \theta)\sqrt{a^2 - b^2}}$
Lame	$\left(\frac{x}{a}\right)^n + \left(\frac{y}{b}\right)^n = 1$	$l = \left(\left \frac{1}{a} \cos \frac{m\theta}{4}\right ^{n_2} + \left \frac{1}{b} \sin \frac{m\theta}{4}\right ^{n_3}\right)^{-\frac{1}{n_1}}$
Cartesian	$\sqrt{x^2 + y^2} + b\sqrt{(x - d)^2 + y^2} = a$	$r^2 - 2(a + b \cos \theta)r + c^2 = 0$
Cassinian	$(x^2 + y^2)^2 - 2a^2(x^2 - y^2) + c^4 = a^4$	$r^4 + a^4 + 2r^2a^2 \cos(2\theta) = c^4$
Pear-shaped	$b^2y^2 = x^3(a - x)^2$	–

$$x_{W_i} = d_{CQ_1} \cos \theta + \sum_{j=1}^i l_{Q_j Q_{j+1}} \cos \phi_j - \frac{1}{2} l_{Q_i Q_{i+1}} \cos \phi_i \tag{3.1}$$

$$y_{W_i} = d_{CQ_1} \sin \theta + \sum_{j=1}^i l_{Q_j Q_{j+1}} \sin(\chi \phi_j) - \frac{1}{2} l_{Q_i Q_{i+1}} \sin \phi_i$$

where $d_{CQ_1} = l$ can be computed based on Table 1 for each constrained trajectory, and the angles θ_i (named absolute angles) are shown in Fig. 2. It can be observed that if all the connecting rods $Q_j Q_{j+1}$, $j = \overline{1, k}$ are constrained by the driver CQ shown in Fig. 1, i.e., $d_{CQ_1} + \sum_{j=1}^k l_{Q_j Q_{j+1}} \leq l_{CQ_1}$, then all the angles ϕ_j , $j = \overline{1, k}$ equal to the angle θ , $\phi_1 = \phi_2 = \dots = \phi_k = \theta$. The velocity vector of the center of mass W_i of each rigid rod $Q_i Q_{i+1}$ of the constrained flexible extensible link is the derivative with respect to time of the position vector \mathbf{r}_{W_i} given by $\mathbf{v}_{W_i} = \dot{\mathbf{r}}_{W_i} = \dot{x}_{W_i} \mathbf{i} + \dot{y}_{W_i} \mathbf{j}$ where

$$v_{x_{W_i}} = \dot{x}_{W_i} = \dot{d}_{CQ_1} \cos \theta - d_{CQ_1} \dot{\theta} \sin \theta - \sum_{j=1}^i l_{Q_j Q_{j+1}} \dot{\phi}_j \sin \phi_j + \frac{1}{2} l_{Q_i Q_{i+1}} \dot{\phi}_i \sin \phi_i \tag{3.2}$$

$$v_{y_{W_i}} = \dot{y}_{W_i} = \dot{d}_{CQ_1} \sin \theta + d_{CQ_1} \dot{\theta} \cos \theta + \sum_{j=1}^i l_{Q_j Q_{j+1}} \dot{\phi}_j \cos \phi_j - \frac{1}{2} l_{Q_i Q_{i+1}} \dot{\phi}_i \cos \phi_i$$

3.1. Dynamic model without clearance

For the model without clearance, the flexible link translates parallel to its support (the rigid guide) and no clearance between the rigid guide and the flexible link is possible. The dynamics of the flexible extensible link can be expressed using the Lagrange differential equation of motion

$$\frac{d}{dt} \left(\frac{\partial T}{\partial \dot{q}_i} \right) - \frac{\partial T}{\partial q_i} = R_i \tag{3.3}$$

where R_i are the generalized forces and $q_i = \theta_i$ are the generalized coordinates, the subscript i represents the number of the generalized forces/coordinates, and where the generalized forces R_i acting on each link can be written as in Dupac and Marghitu (2006). The total kinetic energy of the system in Eq. (3.3) can be expressed as

$$T = \sum_{i=1}^n T_i = \frac{1}{2} \sum_{i=1}^n (m_i \mathbf{v}_{W_i}^2 + I_{W_i} \omega_i^2) \quad (3.4)$$

where T_i is the kinetic energy of each i th component, $I_{W_i} = m(l_{Q_i Q_{i+1}}^2 + h^2)/12$ is the mass moment of inertia with respect to the center of mass W_i of each link and $\boldsymbol{\omega}_i = \omega_i \mathbf{k}$ is the angular velocity and h is the height of the rod i . Equation (3.3) can be expressed in a matrix form by replacing/computing the derivatives inside the equation. A straightforward example for expressing the differential equations of motion in their non-dimensional form can be followed in Awrejcewicz *et al.* (2004).

3.2. Dynamic model with clearance

For the model with clearance, the flexible link of the extensible crank can translate and rotate about its support (rigid guide) as shown in Fig. 5. Due to the clearance model, the flexible link may exhibit impacts on the rigid crank as shown in Fig. 5. To illustrate the impacts of the flexible link with the guide, Fig. 5 was made with a very large backlash in order to make the clearance clearly visible.

The possible impact model for the flexible link is shown in Fig. 5, that is (a) no contact/impact between the moving link and the guide, (b) impact on a single point, and, (c) impact on two points. In the dynamics of the flexible link with impact, the conditions for switching from one impact model to another depends on the initial conditions, on the dynamic response of the system, as well as on the material colliding properties. Since multiple impacts at the same time instant can be statistically excluded, simultaneous impacts on two points are not considered in this study but only presented.

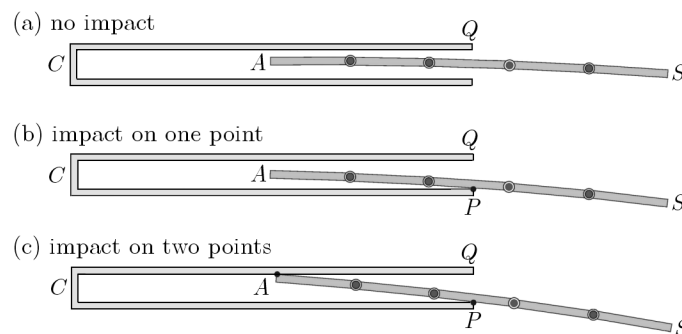


Fig. 5. Constrained flexible extensible link with rigid support and the clearance model, (a) no impact, (b) impact on one point, (c) impact on two points

Different contact force models such as the one discussed in Lankarani and Nikravesh (1990), Flores *et al.* (2010, 2011), may be considered to model the dynamical response of the system. The system dynamics is modelled by introducing the contact force models into the equations of motion as external generalized forces. The equations of motion can be expressed as in Marghitu *et al.* (1999), Dupac and Beale (2010), Flores *et al.* (2011). Considering the contact force components to be elastic and dissipative components, the expression of the contact (impact) force can be expressed as in Lankarani and Nikravesh (1990) by

$$F_n = \kappa \delta^n + D \dot{\delta} \quad (3.5)$$

where $\kappa \delta^n$ represents the elastic force, $D \dot{\delta}$ represents the dissipation of energy during impact, $\kappa \delta$ is a positive real number which specifies the stiffness of the boundary, κ is the stiffness coefficient at the contact interface, δ is the penetration, n is an exponential coefficient, D is the hysteresis as a function of penetration, and $\dot{\delta}$ is the relative impact velocity. Based on the

impact force model with a compliant force formulation (Ryan, 1990) as well as Lankarani and Nikravesh (1990), Stoenescu and Marghitu (2003), Sharf and Zhang (2006), Yang *et al.* (2009), Machado *et al.* (2012), the impact force can be evaluated using Eq. (3.5) by replacing D with the viscous damping coefficient $c(\delta)$ (Ryan, 1990) as

$$F_n = \begin{cases} \kappa\delta^n + c(\delta)\dot{\delta} & \delta > 0 \\ 0 & \delta \leq 0 \end{cases} \quad (3.6)$$

where

$$c(\delta) = \begin{cases} 0 & \delta \leq 0 \\ c_{max} \frac{\delta^2}{d_{max} - \delta} \left(3 - \frac{2\delta}{d_{max} - \delta} \right) & 0 < \delta < d_{max} \\ c_{max} & \delta \geq d_{max} \end{cases}$$

and where d_{max} is the boundary penetration and c_{max} is the maximum value of the damping coefficient.

4. Simulations and results

In this section, results from computer simulations are presented. Simulations have been performed for an extensible link composed of a guide of length $l_{CQ} = 0.11$ m and a flexible link of length $l_{AS} = 0.1$ m. The rotating end C of the guide is located on the Ox axis at 0.03 m from its origin. For the clearance model, the clearance between the guide and the extensible link (one side) was considered to be $5 \cdot 10^{-3}$ m. The clearance was chosen to accentuate the impact effect of the moving part with the guide and to allow a good distinction between the case with and without clearance. The material property for the guide and for the moving part has the density 7850 kg/m^3 , Young's modulus $2 \cdot 10^{11}$ Pa and Poisson's ratio 0.3. The contact stiffness at the contact interface was considered to be 3.52, the exponent coefficient (force exponent) of 2.29 and hysteresis damping coefficient of $2.7 \cdot 10^{10}$. A Gear integrator based on a Backwards Difference Formula (BDF) was used for the integration of the dynamic equations. The BDF scheme using an accurate variable step, variable order integration error, with a step size of 0.001 s and an integration tolerance/error of 0.001 has been considered.

The dynamical behaviour of the extensible crank with a flexible link and clearance constrained to a circular, Cassinian, Cartesian, elliptic, Lamé and a pear-shaped quartic trajectory is shown in Fig. 6, that is, the trajectories of the end S of the constrained extensible link are plotted vs. the crank angle in the polar coordinate system. From Fig. 6 one can observe that the trajectories of the extensible crank with the flexible link and clearance diverge in time, that is, a separation of nearby trajectories and a clear sign of nonlinear motion. Since trajectory divergence is an important factor which affects the dynamics of the extensible link, the behaviour of the extensible crank with the flexible link and clearance vs. rigid link without clearance was considered for the constrained trajectories shown in Fig. 4. It was first observed that the extensible crank with the rigid link and no clearance undergoes periodic motion, that is, stable behaviour.

In order to decide "how much the trajectories of motion" of the flexible link with clearance "resemble" the ones of the rigid link without clearance, the distance between the trajectories has been evaluated using the standard mathematical norm L_2 (Lebedev *et al.*, 2000), i.e., Euclidean norm. The data in Fig. 7 shows the rolling mean divergence between the extensible crank with the flexible link and clearance vs. rigid link and no clearance, evaluated using the mathematical norm L_2 , for all the constrained trajectories shown in Fig. 6. It can be seen that the divergence

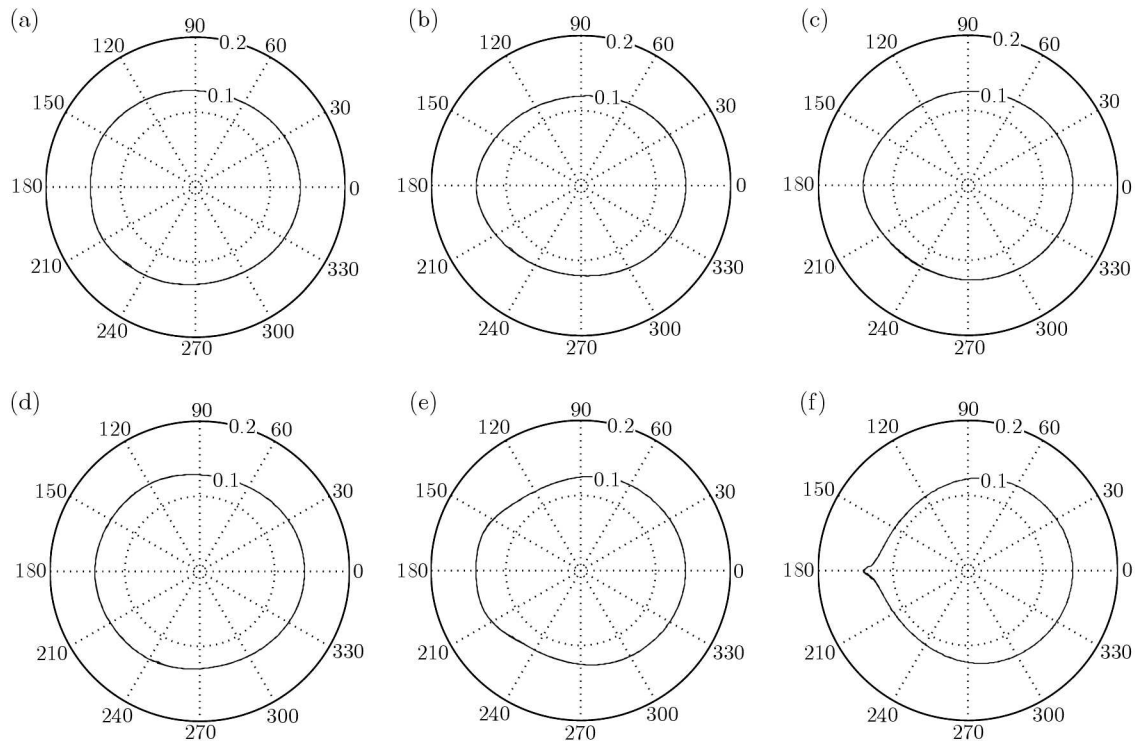


Fig. 6. Polar trajectories of the flexible extensible link following an: (a) Cassinian, (b) Cartesian (also called Descartes), (c) elliptic, (d) circular, (e) Lamé, (f) pear-shaped quartic trajectory

is noisy at the beginning of motion mainly due to the initial conditions. It was observed that the time evolution of the system is affected by clearance and velocity, that is, the combined effect of link flexibility and clearance accentuate trajectory divergence and affect system stability. It was also observed that some of the constrained trajectories (such as the Cartesian and Lamé) can make the system more unstable when the impact (due to clearance) correlates with an increase in trajectory velocity, and others (such as the pear-shaped trajectory) can also increase the instability of the system when the impact (due to clearance) correlates with a sudden change of the trajectory direction.

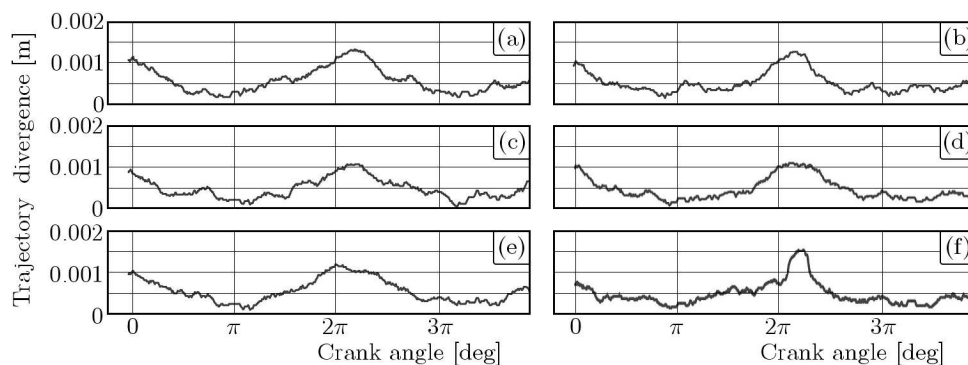


Fig. 7. Divergence d of the trajectories of motion (measured using the mathematical norm L_2) between the extensible crank with the flexible link and clearance vs. rigid link without clearance plotted vs. the crank angle for, (a) Cartesian, (b) circular, (c) Cassinian, (d) Lamé, (e) elliptic, (f) pear-shaped quartic trajectory

It can be seen in Fig. 7 that less resemblance between the trajectories of motion is for the Cartesian, Lamé and pear-shaped quartic trajectory. Since the Lamé trajectory shows clear

dynamical behaviour “divergence” signs, that is, less resemblance with the stable trajectory of the rigid extensible link, a further analysis of the behaviour of this type of constrained flexible link for different stiffness values and angular velocities have been considered.

Considering no changes in the parameters of the dynamical simulation, the trajectories of the end of the extensible flexible link (Ox -(1) and Oy -(2) trajectories) and the phase diagram (position vs. velocity) are plotted in Fig. 8.

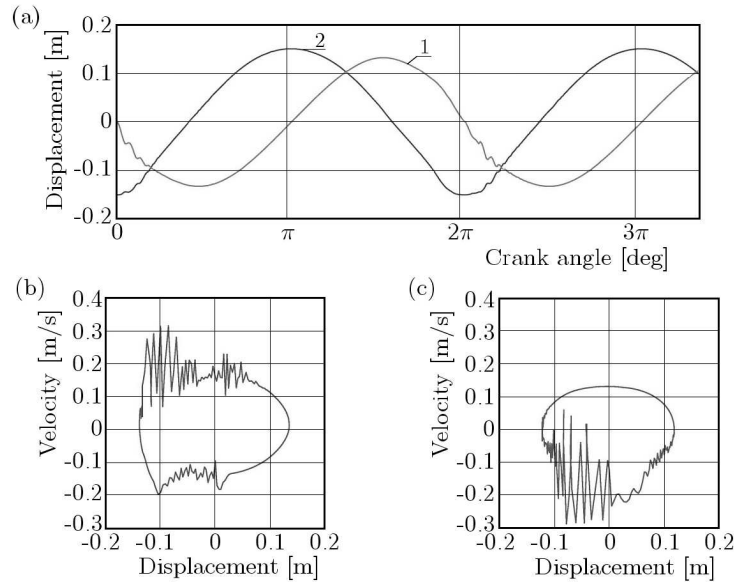


Fig. 8. Dynamical behaviour of the active end of the extensible flexible link for a constrained Lame trajectory; (a) Ox (1) and Oy (2) trajectories plotted vs. the crank angle, (b) Ox velocity vs. position, and (c) Oy velocity vs. position

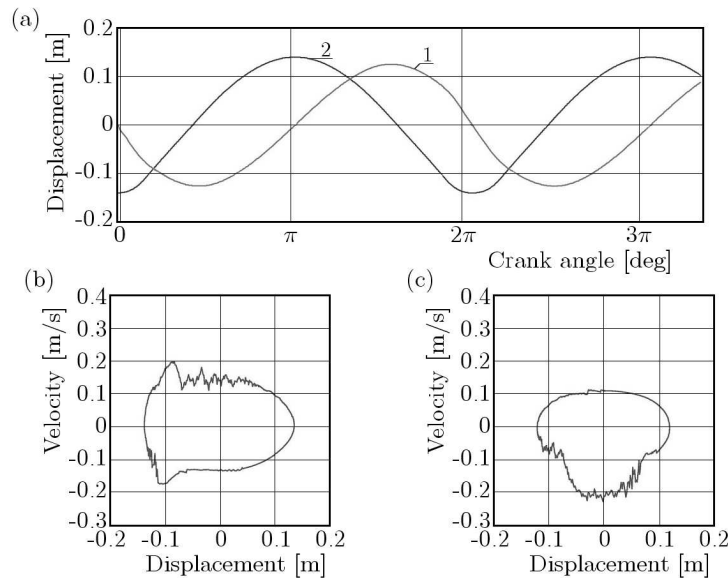


Fig. 9. Dynamical behaviour of the active end of the extensible flexible link for a constrained Lame trajectory. (a) Ox (1) and Oy (2) trajectories plotted vs. the crank angle, (b) Ox velocity vs. position, and (c) Oy velocity vs. position

To gain more insight into the system behaviour, the velocity and displacement amplitude of the active end of the flexible link have been plotted for a stiffer link. The trajectories of motion and phase diagram (position vs. velocity) of the end of the extensible flexible link computed

for springs with the spring constant values ten times higher than before (Fig. 8) are shown in Fig. 9. The result of this change in stiffness is an increase in the amplitude of oscillations of the active end of the flexible link velocity as well as an increase in the link deflection amplitude. This clearly shows the nonlinear effect on the deflection of the link due to stiffness as well as the effect of clearance between the flexible link and guide, that is, suddenly changes of the velocity and direction of motion due to impacts.

Finally, one can observe that a more complex behaviour of the flexible link can occur when the angular velocity of the rotating link changes. Increasing ten times the angular velocity (for the same link stiffness as in Fig. 8), the phase diagram (position vs. velocity) as well as the Ox (1) and Oy (2) trajectories shown in Fig. 10 are obtained. Figure 10 clearly shows an increase in the velocity amplitude of the active end of the flexible link due to the increased angular velocity, but small deflection on the trajectories of motion. One can summarize that both link stiffness and angular velocity plays an important role in the dynamical behaviour and stability of the considered mechanical system.

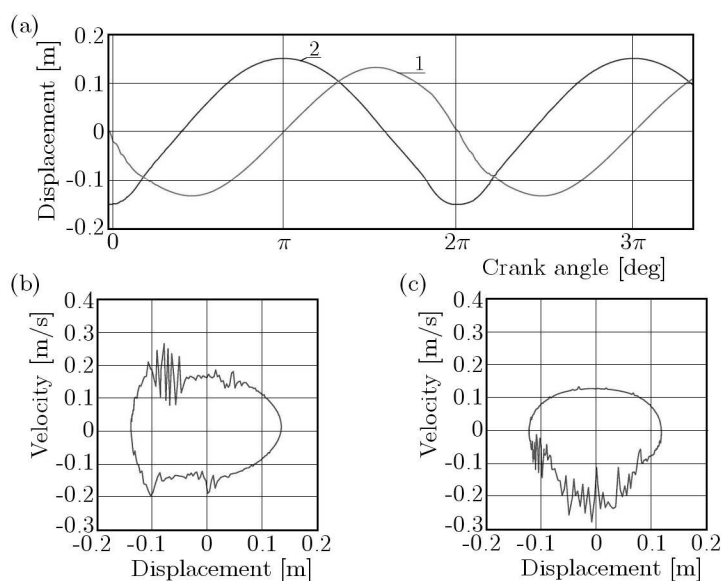


Fig. 10. Dynamical behaviour of the active end of the extensible flexible link for a constrained Lamé trajectory. (a) Ox (1) and Oy (2) trajectories plotted vs. the crank angle, (b) Ox velocity vs. position, and (c) Oy velocity vs. position

5. Conclusions

In this paper, the modelling of an extensible crank mechanism with a constrained flexible link and a rigid crank is presented and its behaviour analysed. Accurate simulation, for the constrained circular, Cartesian, elliptical, Cassinian, Lamé and pear-shaped quartic trajectories are performed. A dynamical analysis is carried out in order to compare the dynamical response of the flexible link vs. the rigid link under the combined effect of the clearance and impact. Periodic motion was observed for dynamics of the constrained rigid link and no clearance. A clear divergence of the trajectories was observed for the constrained extensible mechanism with a flexible link and clearance. Moreover, some of the constrained trajectories make the system more unstable when the impact due to clearance correlates with an increase in the velocity or with a suddenly change of the constrained curve direction. It was concluded that the parameters such as clearance, rotational velocity and trajectories constraints should not be ignored when analysing mechanical systems performance and stability. Furthermore, experimental tests with different materials will be performed in order to generalize the simulations reported in the paper.

References

1. AWREJCEWICZ J., KUDRA G., LAMARQUE C.-H., 2004, Investigation of triple physical pendulum with impacts using fundamental solution matrices, *International Journal of Bifurcation and Chaos*, **14**, 12, 4191-4213
2. BEALE D., LEE S.W., BOGHIU D., 1998, An analytical study of fuzzy control of a flexible rod mechanism, *Journal of Sound and Vibration*, **210**, 1, 37-52
3. BOGHIU D., MARGHITU D., SINHA S.C., 1996, Stability and control of a parametrically excited rotating beam, *6th Conference on Nonlinear Vibrations, Stability and Dynamics of Structures*, 163-169
4. BRACH R.M., 1989, Rigid body collisions, *Journal of Applied Mechanics*, **56**, 133-138
5. DUPAC M., 2013, A virtual prototype of a constrained extensible crank mechanism: dynamic simulation and design, *Proceedings of the Institution of Mechanical Engineers, Part K: Journal of Multi-Body Dynamics*, **227**, 3, 201-210
6. DUPAC M., 2012, The dynamics of an extensible link with one and two moving ends, *Annals of University of Craiova, Mathematics and Computer Science Series*, **39**, 1, 48-54
7. DUPAC M., BEALE D.G., 2010, Dynamic analysis of a flexible linkage mechanism with cracks and clearance, *Mechanism and Machine Theory*, **45**, 12, 1909-1923
8. DUPAC M., MARGHITU D.B., 2006, Nonlinear dynamics of a flexible mechanism with impact, *Journal of Sound and Vibration*, **289**, 952-966
9. FILIPICH C. P., ROSALES M.B., 2000, A further study on the post buckling of extensible elastic rods, *International Journal of Non-Linear Mechanics*, **35**, 997-1022
10. FLORES P., LEINE R., GLOCKER C., 2010, Modeling and analysis of planar rigid multibody systems with translational clearance joints based on the non-smooth dynamics approach, *Multibody System Dynamics*, **23**, 165-190
11. FLORES P., MACHADO M., SILVA M.T., MARTINS J.M., 2011, On the continuous contact force models for soft materials in multibody dynamics, *Multibody System Dynamics*, **25**, 357-375
12. FRITZKOWSKI P., KAMINSKI H., 2009, Dynamics of a rope modeled as a discrete system with extensible members, *Computational Mechanics*, **44**, 473-480
13. GARCIA J., BAYO J.E., 1994, *Kinematic and Dynamic Simulation of Multibody Systems*, Springer, New York
14. IZUMI T., HITAKA Y., 1993, Control of impact for a hammering robot using a flexible link, [In:] *Robotics, Mechatronics and Manufacturing Systems*, Takamori T., Tsuchiya K. (Edit.), Elsevier, 327-332
15. JIN C., FAN L., QIU Y., 2004, The vibration control of a flexible linkage mechanism with impact, *Communications in Nonlinear Science and Numerical Simulation*, **9**, 459-469
16. KHEMILI I., ROMDHANE L., 2008, Dynamic analysis of a flexible slider-crank mechanism with clearance, *European Journal of Mechanics A/Solids*, **27**, 882-898
17. KVECSES, J., CLEGHORN, W. L., 2004, Impulsive dynamics of a flexible arm: analytical and numerical solutions, *Journal of Sound and Vibration*, **269**, 12, 183-195
18. LANKARANI H.M., NIKRAVESH P.E., 1990, A contact force model with hysteresis damping for impact analysis of multibody systems, *Journal of Mechanical Design*, **112**, 369-376
19. LEBEDEV L.P., VOROVICH I. I., GLADWELL G.M.L., 2000, *Functional Analysis: Applications in Mechanics and Inverse Problems*, Kluwer Academic Publishers, Dordrecht
20. LEE S.Y., SHEU J.J., 2007, Free vibration of an extensible rotating inclined Timoshenko beam, *Journal of Sound and Vibration*, **304**, 606-624

21. LIU S., WU L., LU Z., 2007, Impact dynamics and control of a flexible dual-arm space robot capturing an object, *Applied Mathematics and Computation*, **185**, 2, 1149-1159
22. MACHADO M., MOREIRA P., FLORES P., LANKARANI H.M., 2012, Compliant contact force models in multibody dynamics: Evolution of the Hertz contact theory, *Mechanism and Machine Theory*, **53**, 99-121
23. MARGHITU D.B., SINHA S.C., DIACONESCU C., 1999, Control of a parametrically excited flexible beam undergoing rotations and impacts, *Multibody System Dynamics*, **3**, 47-63
24. MITIGUY P., BANERJEE A.K., 2000, Determination of spring constants for modeling flexible beams, Working Model Technical Paper
25. RUBINSTEIN D., 1999, Dynamics of a flexible beam and a system of rigid rods, with fully inverse (one-sided) boundary conditions, *Computational Methods Applied Mechanical Engineering*, **175**, 87-97
26. RYAN R.R., 1990, *ADAMS-Multibody System Analysis Software*, *Multibody Systems Handbook*, Springer-Verlag, Berlin
27. SHARF I., ZHANG Y., 2006, A contact force solution for non-colliding contact dynamics simulation, *Multibody System Dynamics*, **16**, 263-290
28. STOENESCU E. D., MARGHITU D.B., 2003, Dynamic analysis of a planar rigid-link mechanism with rotating slider joint and clearance, *Journal of Sound and Vibration*, **266**, 394-404
29. YANG Y., REN W., CHEN L., JIANG M., YANG Y., 2009, Study on ride comfort of tractor with tandem suspension based on multi-body system dynamics, *Applied Mathematical Modelling*, **33**, 11-33
30. ZHANG D.-G., ANGELES J., 2005, Impact dynamics of flexible-joint robots, *Computers and Structures*, **83**, 1, 25-33
31. ZHUANG F., WANG Q., 2012, Modeling and simulation of the nonsmooth planar rigid multibody systems with frictional translational joints, *Multibody System Dynamics*, <http://link.springer.com/article/10.1007/s11044-012-9328-5>

Manuscript received April 30, 2013; accepted for print February 4, 2014